

# Recent results from the KEDR Detector <sup>\*</sup>

V.V. Anashin<sup>1</sup>, V.M. Aulchenko<sup>1,2</sup>, E.M. Baldin<sup>1,2</sup>, A.K. Barladyan<sup>1</sup>, A.Yu. Barnyakov<sup>1</sup>, M.Yu. Barnyakov<sup>1</sup>, S.E. Baru<sup>1,2</sup>, I.V. Bedny<sup>1</sup>, O.L. Beloborodova<sup>1,2</sup>, A.E. Blinov<sup>1,1)</sup>, V.E. Blinov<sup>1,3</sup>, A.V. Bobrov<sup>1</sup>, V.S. Bobrovnikov<sup>1</sup>, A.V. Bogomyagkov<sup>1,2</sup>, A.E. Bondar<sup>1,2</sup>, A.R. Buzykaev<sup>1</sup>, S.I. Eidelman<sup>1,2</sup>, Yu.M. Glukhovchenko<sup>1</sup>, V.V. Gulevich<sup>1</sup>, D.V. Gusev<sup>1</sup>, S.E. Karnaev<sup>1</sup>, S.V. Karpov<sup>1</sup>, T.A. Kharlamova<sup>1,2</sup>, V.A. Kiselev<sup>1</sup>, S.A. Kononov<sup>1,2</sup>, K.Yu. Kotov<sup>1</sup>, E.A. Kravchenko<sup>1,2</sup>, V.F. Kulikov<sup>1,2</sup>, G.Ya. Kurkin<sup>1,3</sup>, E.A. Kuper<sup>1,2</sup>, E.B. Levicev<sup>1,3</sup>, D.A. Maksimov<sup>1</sup>, V.M. Malyshev<sup>1</sup>, A.L. Maslennikov<sup>1</sup>, A.S. Medvedko<sup>1,2</sup>, O.I. Meshkov<sup>1,2</sup>, S.I. Mishnev<sup>1</sup>, I.I. Morozov<sup>1,2</sup>, N.Yu. Muchnoi<sup>1,2</sup>, V.V. Neufeld<sup>1</sup>, S.A. Nikitin<sup>1</sup>, I.B. Nikolaev<sup>1,2</sup>, I.N. Okunev<sup>1</sup>, A.P. Onuchin<sup>1,3</sup>, S.B. Oreshkin<sup>1</sup>, I.O. Orlov<sup>1,2</sup>, A.A. Osipov<sup>1</sup>, S.V. Peleganchuk<sup>1</sup>, S.G. Pivovarov<sup>1,3</sup>, P.A. Piminov<sup>1</sup>, V.V. Petrov<sup>1</sup>, A.O. Poluektov<sup>1</sup>, I.N. Popkov<sup>1</sup>, V.G. Prisekin<sup>1</sup>, A.A. Ruban<sup>1</sup>, V.K. Sandyrev<sup>1</sup>, G.A. Savinov<sup>1</sup>, A.G. Shamov<sup>1</sup>, D.N. Shatilov<sup>1</sup>, B.A. Shwartz<sup>1,2</sup>, E.A. Simonov<sup>1</sup>, S.V. Sinyatkin<sup>1</sup>, Yu.I. Skovpen<sup>1,2</sup>, A.N. Skrinsky<sup>1</sup>, V.V. Smaluk<sup>1,2</sup>, A.V. Sokolov<sup>1</sup>, A.M. Sukharev<sup>1</sup>, E.V. Starostina<sup>1,2</sup>, A.A. Talyshev<sup>1,2</sup>, V.A. Tayursky<sup>1</sup>, V.I. Telnov<sup>1,2</sup>, Yu.A. Tikhonov<sup>1,2</sup>, K.Yu. Todyshev<sup>1,2</sup>, G.M. Tumaikin<sup>1</sup>, Yu.V. Usov<sup>1</sup>, A.I. Vorobiov<sup>1</sup>, A.N. Yushkov<sup>1</sup>, V.N. Zhilich<sup>1</sup>, V.V. Zhulanov<sup>1,2</sup>, A.N. Zhuravlev<sup>1,2</sup>

1 (Budker Institute of Nuclear Physics, 11, Lavrentiev prospect, Novosibirsk, 630090, Russia)

2 (Novosibirsk State University, 2, Pirogova street, Novosibirsk, 630090, Russia)

3 (Novosibirsk State Technical University, 20, Karl Marx prospect, Novosibirsk, 630092, Russia)

**Abstract** We report results of experiments performed with the KEDR detector at the VEPP-4M  $e^+e^-$  collider. They include precise measurement of the  $D^0$  and  $D^\pm$  meson masses, determination of the  $\psi(3770)$  resonance parameters, and a search for narrow resonances in  $e^+e^-$  annihilation at center-of-mass energies between 1.85 and 3.1 GeV.

**Key words**  $D$  meson,  $\psi(3770)$ , mass, narrow resonances

**PACS** 13.20.Fc, 13.20.Gd, 13.66.Bc, 14.40.Lb, 14.40.Rt

## 1 Introduction

The paper reports results of three analyses performed with the KEDR detector at the VEPP-4M collider (BINP, Novosibirsk): a measurement of  $D^0$  and  $D^\pm$  meson masses, a measurement of  $\psi(3770)$  mass and widths, and a search for narrow resonances in  $e^+e^-$  annihilation between 1.85 and 3.1 GeV.

## 2 VEPP-4M collider and KEDR detector

The VEPP-4M collider [1] can operate in the wide range of beam energy from  $2E = 2$  to 12 GeV. The peak luminosity in the  $J/\psi$  energy region is about  $2 \times 10^{30} \text{ cm}^{-2} \text{ s}^{-1}$ . One of the main features of

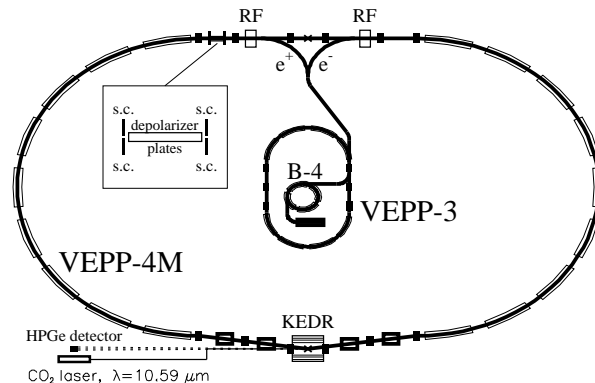


Fig. 1. VEPP-4M/KEDR complex with the resonant depolarization and the infrared light Compton backscattering facilities.

<sup>\*</sup> Partially supported by the Russian Foundation for Basic Research, Grant 04-02-16712, 07-02-00816, 07-02-01162 and RF Presidential Grant for Sc. Sch. NSh-5655.2008.2

1) E-mail: A.E.Blinov@inp.nsk.su

the VEPP-4M is its capability to precisely measure the beam energy using two techniques [2]: resonant depolarization and infrared light Compton backscattering.

The accuracy of VEPP-4M energy measurement with the resonant depolarization reaches  $10^{-6}$ . Such measurement requires dedicated calibration runs without data taking. The accuracy of the beam energy determination for the accumulated data sample is dominated by the interpolation between the successive depolarization runs and equals about  $6 \cdot 10^{-6}$  ( $\simeq 10$  keV) in the  $J/\psi$  region [3].

A new technique developed at the BESSY-I and BESSY-II synchrotron radiation sources [4, 5] was adopted for VEPP-4M in 2005. It employs the infrared light Compton backscattering and has a worse precision compared to the resonant depolarization (50 ÷ 70 keV in the  $J/\psi$  region), but unlike the latter it can be used during data taking [2].

The KEDR detector [6] includes the vertex detector, the drift chamber, the scintillation time-of-flight counters, the aerogel Cherenkov counters, the barrel liquid krypton calorimeter, the endcap CsI calorimeter, and the muon system embedded in the yoke of a superconducting coil generating a field of 0.6 T. The detector also includes a high-resolution tagging system for studies of two-photon processes. The on-line luminosity measurement is performed with two independent single bremsstrahlung monitors.

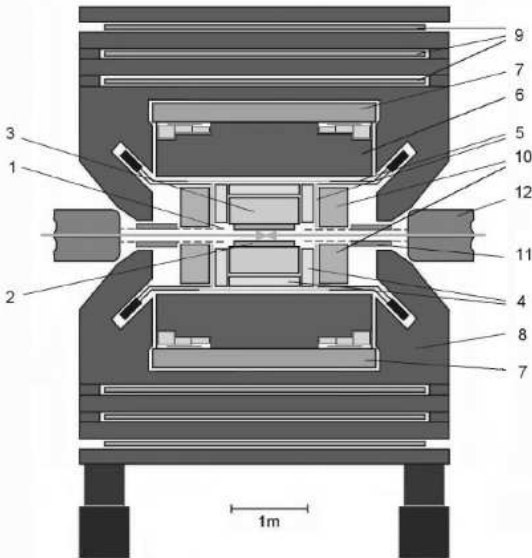


Fig. 2. KEDR detector. 1-vacuum chamber, 2-vertex detector, 3-drift chamber, 4-threshold aerogel counters, 5-ToF-counters, 6-liquid krypton calorimeter, 7-superconducting coil (0.6 T), 8-magnet yoke, 9-muon tubes, 10-CsI-calorimeter, 11-compensation solenoid, 12-VEPP-4M quadrupole.

### 3 $D^0$ and $D^\pm$ meson masses

Neutral and charged  $D$  mesons are the ground states in the family of open charm mesons. Measurement of their masses provides a mass scale for the heavier excited states. In addition, a precise measurement of the  $D^0$  meson mass could help to understand the nature of the narrow  $X(3872)$  state [7–10], which, according to some models, is a bound state of  $D^0$  and  $D^{*0}$  [11] mesons and has a mass very close to the sum of the  $D^0$  and  $D^{*0}$  meson masses.

Measurement of  $D$  meson masses is performed using the near-threshold  $e^+e^- \rightarrow D\bar{D}$  production at the  $\psi(3770)$  resonance with the full reconstruction of one of the  $D$  mesons. Neutral and charged  $D$  mesons are reconstructed in the  $K^-\pi^+$  and  $K^-\pi^+\pi^+$  final states, respectively (charge-conjugate states are implied throughout this paper). The analysis uses a data sample of  $0.9 \text{ pb}^{-1}$ .

The mass of the  $D$  meson is calculated as

$$M_{bc} \simeq \sqrt{E_{\text{beam}}^2 - \left( \sum_i \vec{p}_i \right)^2}, \quad (1)$$

(so-called *beam-constrained mass*), where  $E_{\text{beam}}$  is the average energy of colliding beams and  $\vec{p}_i$  are the momenta of the  $D$  decay products. Since  $E_{\text{beam}}$  is measured by resonant depolarization technique as described in Sec. 2, its contribution to the  $D$  mass error is negligible.

Apart of the  $M_{bc}$ ,  $D$  decays are effectively selected by energy difference

$$\Delta E = \sum_i \sqrt{M_i^2 + p_i^2} - E_{\text{beam}} \quad (2)$$

where  $M_i$  and  $p_i$  are the masses and momenta of the  $D$  decay products. The signal events satisfy a  $\Delta E \simeq 0$  condition. Therefore, the scale of momenta is tuned in order to get  $\langle \Delta E \rangle$  of  $D$  decays consistent with zero. Furthermore, while calculating  $M_{bc}$ , we employ a kinematic fit with the  $\Delta E = 0$  constraint. It results in a certain improvement of the  $M_{bc}$  resolution and significantly reduces a contribution of the remaining momentum scale error to the measured  $D$  mass.

In order to measure the  $D$  mass most efficiently, the unbinned maximum likelihood fit procedure is used. In the case of  $D^+$  meson analysis, the likelihood function depends on two already defined variables:  $M_{bc}$  and  $\Delta E$ . The  $D^0$  meson analysis employs one more variable: the difference of the absolute values of momenta of  $D^0$  decay products in the CM frame  $\Delta|p|$ . We use the fact that the  $M_{bc}$  resolution strongly depends on decay kinematics — it is

about three times better if daughter particles move transversely to the  $D^0$  direction (small  $\Delta|p|$ ), than if they move along this direction (large  $\Delta|p|$ ). Thus, the  $\Delta|p|$  variable estimates the  $M_{bc}$  resolution on the event-by-event basis, improving the overall statistical accuracy of the measurement.

A fit of the event density is performed with  $D$  mass as one of the parameters in a relatively wide region around  $M_{bc} = M_D$  and  $\Delta E = 0$  (specifically,  $M_{bc} > 1700$  MeV,  $|\Delta E| < 300$  MeV), with the background contribution taken into account. The likelihood function has the form:

$$-2 \log \mathcal{L}(\alpha) = -2 \sum_{i=0}^N \log p(\mathbf{v}_i | \alpha) + 2N \log \int p(\mathbf{v} | \alpha) d\mathbf{v} \quad (3)$$

where  $\mathbf{v} = (M_{bc}, \Delta E, \Delta|p|)$  are the variables that characterize one event,  $p(\mathbf{v} | \alpha)$  is the probability distribution function (PDF) of these variables depending on the fit parameters  $\alpha = (M_D, \langle \Delta E \rangle, b_{uds}, b_{DD})$ :

$$p(\mathbf{v} | \alpha) = p_{sig}(\mathbf{v} | M_D, \langle \Delta E \rangle) + b_{uds} p_{uds}(\mathbf{v}) + b_{DD} p_{DD}(\mathbf{v}). \quad (4)$$

Here  $p_{sig}$  is the PDF of the signal events which depends on  $M_D$  and  $\langle \Delta E \rangle$  (the central value of the  $\Delta E$  distribution),  $p_{uds}$  is the PDF for the background process  $e^+e^- \rightarrow q\bar{q}$  ( $q = u, d, s$ ), and  $p_{DD}$  is the PDF for the background from  $e^+e^- \rightarrow D\bar{D}$  decays with  $D$  decaying to all modes other than the signal one.  $b_{uds}$  and  $b_{DD}$  are relative magnitudes of the background terms. The shapes of the  $p_{sig}$ ,  $p_{uds}$  and  $p_{DD}$  distributions are obtained from the MC simulation.

The simulation of signal events is performed with the MC generator for  $e^+e^- \rightarrow D\bar{D}$  decays where  $D$ -meson decays are simulated by the JETSET 7.4 package [12]. The radiative corrections are taken into account in both initial (the RADCOR package [13] with Kuraev-Fadin model [21]), and final states (the PHOTOS package [14]). The ISR corrections use the  $e^+e^- \rightarrow \psi(3770) \rightarrow D\bar{D}$  cross section according to a Breit-Wigner amplitude with  $M = 3771$  MeV and  $\Gamma = 23$  MeV [15]. The backgrounds from the continuum  $e^+e^- \rightarrow q\bar{q}$  process and from  $e^+e^- \rightarrow D\bar{D}$  decays are simulated using the JETSET 7.4 generator. In the latter case the signal  $D$  decays are removed from the decay table. Full simulation of the KEDR detector is performed using the GEANT 3.21 package [16].

The likelihood fits yield  $M_{D^0} = 1865.05 \pm 0.33$  MeV and  $M_{D^+} = 1869.58 \pm 0.49$  MeV. To obtain the final  $D$  masses, one has to account for a possible deviation of the fit parameters  $M_D$  and  $\langle \Delta E \rangle$  from the true  $D$  masses and energies. In particular, the central value of  $M_D$  can be shifted due to the asymmet-

ric resolution function and radiative corrections. The biases are corrected using the MC simulation. The final values of the  $D$  masses after the corrections are  $M_{D^0} = 1865.30 \pm 0.33$  MeV and  $M_{D^+} = 1869.53 \pm 0.49$  MeV, where the errors are statistical only.

	$\Delta M_{D^0}$ , MeV	$\Delta M_{D^+}$ , MeV
Absolute momentum calibration	0.04	0.04
Ionization loss in the material	0.01	0.03
Momentum resolution	0.13	0.10
ISR corrections	0.16	0.11
Signal PDF	0.07	0.05
Continuum background PDF	0.04	0.09
$D\bar{D}$ background PDF	0.03	0.06
Beam energy calibration	0.01	0.01
Total	0.23	0.20

Table 1. Systematic uncertainties in the  $D^0$  and  $D^+$  mass measurements.

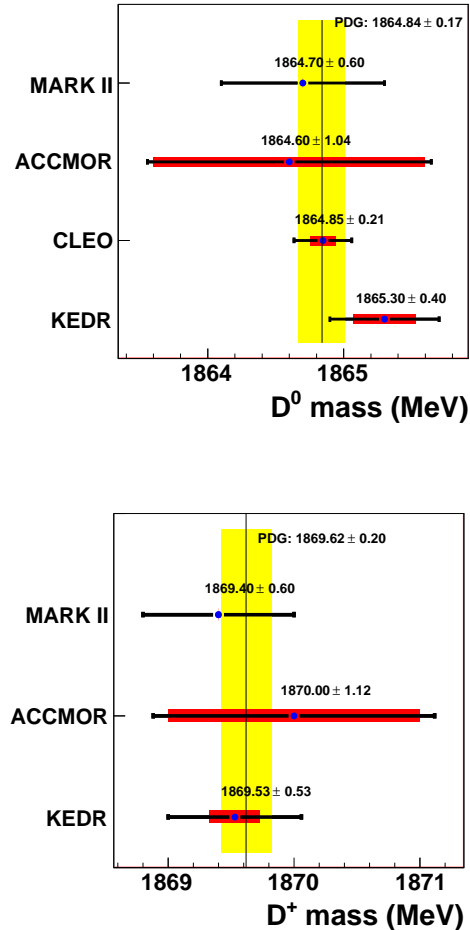


Fig. 3. Comparison of KEDR  $D$  meson masses with other measurements. The thick and thin error bars show the systematic and the total errors, respectively. The shaded areas are the PDG-2008 values [17]. The PDG value for the  $D^+$  is obtained using the measured mass difference of the  $D^+$  and  $D^0$  mesons.

Estimates of systematic uncertainties in the  $D$  mass measurements are shown in Table 1. Figure 3 shows the comparison of our results with those of the previous experiments.

#### 4 $\psi(3770)$ mass and widths

The parameters of the  $\psi(3770)$  meson were measured in the scans of the broad energy region from the  $\psi'$  mass to 3.95 GeV. The analysis is based on the luminosity integral of about  $2.4 \text{ pb}^{-1}$ .

Following the similar analyses done previously [18, 19], we parameterize tree-level cross sections of non-resonant  $D\bar{D}$  production and  $\psi(3770)$  resonance as:

$$\sigma_{D\bar{D}}^{\text{nonres}}(W) = \sigma^0(W) + \sigma^\pm(W), \quad (5)$$

where  $\sigma^{0,\pm}(W) = \sigma_{D\bar{D}} \cdot \beta_{D^{0,\pm}}^3$ , and

$$\sigma_{\psi(3770)}(W) = \frac{3\pi}{M^2} \frac{\Gamma_{ee}\Gamma_h}{(W-M)^2 + \Gamma^2(W)/4}, \quad (6)$$

where  $M$  is the  $\psi(3770)$  mass,

$$\Gamma(W) = \Gamma_{\text{tot}} \frac{\frac{(R_0 * P_{D_0}(W))^3}{1+(R_0 * P_{D_0}(W))^2} + \frac{(R_0 * P_{D_\pm}(W))^3}{1+(R_0 * P_{D_\pm}(W))^2}}{\frac{(R_0 * P_{D_0}(M))^3}{1+(R_0 * P_{D_0}(M))^2} + \frac{(R_0 * P_{D_\pm}(M))^3}{1+(R_0 * P_{D_\pm}(M))^2}},$$

$\Gamma_{\text{tot}}$  is the  $\psi(3770)$  width, and  $R_0$  is the interaction radius.

The previous experiments [18, 19] have ignored the interference between the  $\psi(3770)$  decay and non-resonant  $D\bar{D}$  production. To investigate its impact on the extracted parameters of the  $\psi(3770)$ , we parameterized the total  $D\bar{D}$  cross section  $\sigma_{D\bar{D}}$  without and with the interference as:

$$\sigma_{D\bar{D}}(W) = \sigma_{\psi(3770)}(W) + \sigma_{D\bar{D}}^{\text{nonres}}(W) \quad (7)$$

and

$$\sigma_{D\bar{D}}(W) = |A_{\psi(3770)}(W) + A_{D\bar{D}}^{\text{nonres}}(W) \cdot e^{i\phi}|^2, \quad (8)$$

respectively, where  $|A_{\psi(3770)}(W)|^2 = \sigma_{\psi(3770)}(W)$ ,  $A_{D\bar{D}}^{\text{nonres}}(W) = \sqrt{\sigma_{D\bar{D}}^{\text{nonres}}(W)}$ , and  $\phi$  is the interference phase.

Parameterization of observable cross section is obtained by convolution of the  $\sigma_{D\bar{D}}(W)$  and  $\psi'$  cross sections with the ISR correction function [21] and beam energy spread similarly to Eq. (9).

Fig. 4 shows the fits of observable cross section without and with the interference. The quality of the latter fit is significantly better (addition of one fit parameter decreases  $\chi^2$  by  $\simeq 8$ ) and the phase  $\phi$  is consistent with  $\pi$ . The preliminary results for the  $\psi(3770)$  parameters are

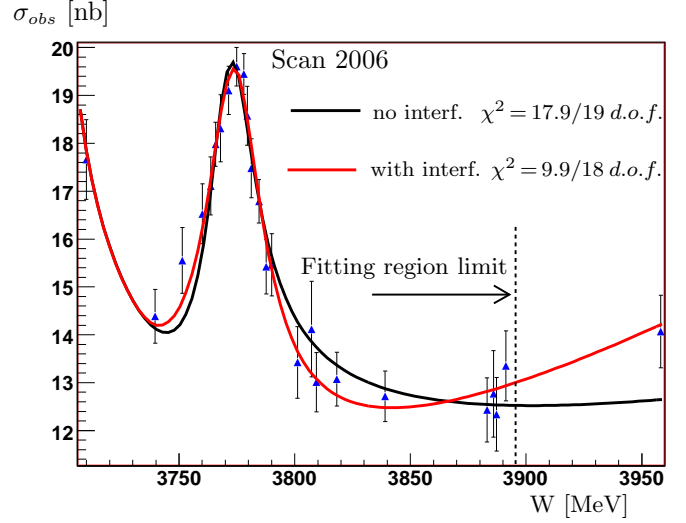


Fig. 4. Fits of observable cross section in the  $\psi(3770)$  region: without and with the interference.

- $M = 3773.2 \pm 0.5 \pm 0.6 \text{ MeV}$ ,
- $\Gamma_{\text{tot}} = 23.9 \pm 2.2 \pm 1.1 \text{ MeV}$ .
- $\Gamma_{ee} = 294 \pm 22 \pm 30 \text{ eV}$ .

for the fit without interference, and

- $M = 3777.8 \pm 1.1 \pm 0.7 \text{ MeV}$ ,
- $\Gamma_{\text{tot}} = 28.2 \pm 3.1 \pm 2.4 \text{ MeV}$ .
- $\Gamma_{ee} = 312 \pm 31 \pm 30 \text{ eV}$ .

for the fit with interference. Significant increase of  $\psi(3770)$  mass in the latter case is apparent.

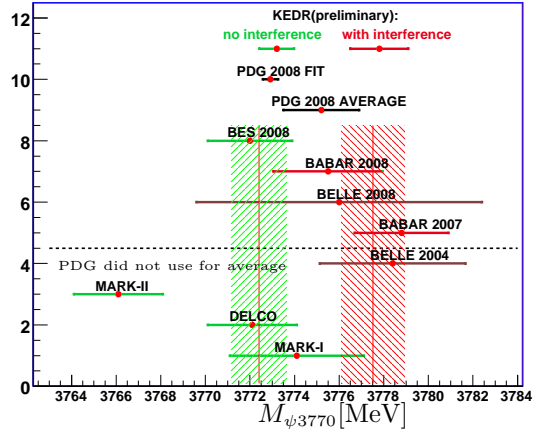


Fig. 5. Comparison of the  $\psi(3770)$  mass measured by KEDR with other experiments.

Figure 5 shows comparison of KEDR  $\psi(3770)$  masses with results of other experiments. Mass from our non-interference fit is consistent with other measurements, which ignore the interference, while mass

from the interference fit is consistent with the BaBar results [20] which also takes the interference into account.

## 5 Search for narrow resonances

After the  $J/\psi$  discovery, search for other narrow resonances was performed by several experiments. The energy region between  $J/\psi$  and  $\Upsilon$  mesons was explored by MARK-1 at SPEAR [22], LENA at DORIS [23], and MD-1 at VEPP-4 [24]. The upper limit on the leptonic width of narrow resonances obtained in these analyses varies between 15 and 970 eV depending on energy. The search in the energy region below  $J/\psi$  mass and down to 1.91 GeV was performed only in experiments at ADONE [25, 26] with the upper limit about 500 eV. Recently KEDR collaboration has revisited the latter region in view of a recent discovery of unexpected exotic states above the charm threshold, including the narrow  $X(3872)$  state, which proved that surprises are still possible even at low energies.

### 5.1 Experiment description

The experiment was performed in the beginning of 2009 and the results are very preliminary. The energy scan started just above  $J/\psi$  and finished at 1.85 GeV. The search for narrow resonances was conducted by automatic decrease of the center-of-mass energy by about  $2\sigma_w$  (1.4 to 1.9 MeV) steps after collection of required integrated luminosity in each point. The integrated luminosity per energy point varied from  $0.3 \text{ nb}^{-1}$  in the upper part of the energy range to  $0.12 \text{ nb}^{-1}$  in the lower one. The data taken at each energy were analyzed in real time. In order to improve sensitivity, the integrated luminosity was doubled in the energy points with significant excess of candidate events.

The total integrated luminosity of  $\simeq 0.28 \text{ pb}^{-1}$  was collected. The luminosity for data taking was monitored using the process of single bremsstrahlung, while the analysis uses the offline measurement based on elastic  $e^+e^-$  scattering in the endcap calorimeter. The beam energy was measured by the Compton backscattering technique described in Sec. 2

### 5.2 Data analysis

The analysis employs three sets of event selection criteria with the efficiency to hadronic  $J/\psi$  decays ( $\varepsilon_h$ ) varying from 44% to 65%. The  $\varepsilon_h$  was measured from the observable  $J/\psi$  cross section and known  $\Gamma_{ee}^{J/\psi} \cdot Br(J/\psi \rightarrow hadr)$ . Below we describe the soft-

est set of event selection criteria. At the first stage we defined track-level criteria to select good charged tracks:

1. Distances of closest approach to the beam in the transverse plane and along the beam axis are less than 0.5 and 10 cm, respectively;
2. The deposited energy in the barrel LKr calorimeter is above 20 MeV.

Then an event-level selection, which account a calorimeter objects too, was applied:

1. The total deposited energy in the calorimeter is above 400 MeV;
2. At least two charged tracks in the event satisfy first criteria of the track-level selection;
3. At least one “good” charged track satisfies both track-level criteria;
4. There is a charged track acoplanar to the “good” one:  $|\Delta\phi - \pi| > 0.15 \text{ rad}$ ;
5. Aplanarity of event (sum of momenta transverse to “event plane”) is above  $0.1 \cdot E_{beam}$
6. There are less than 4 hits in the Muon Chambers;
7.  $|\sum p_i^z / \sum E_i| < 0.5$ .

Condition 4 rejects cosmic rays, Bhabhas, and dimuon events. Condition 5 rejects radiative Bhabhas and dimuons. Condition 6 rejects cosmic ray showers. Condition 7 rejects two-photon processes and hard ISR.

### 5.3 Fit results

The event yield depending on energy is fitted by a function that assumes the existence of a resonance with mass  $M_R$ , the leptonic width  $\Gamma_{ee}^R$ , and selection efficiency  $\varepsilon_h$  on top of flat nonresonant background. The following parameterization of the observable cross section was used:

$$\sigma(W) = \sigma_0 + \varepsilon_h \int dW' dx \sigma_{R \rightarrow hadr}(W') \cdot \mathcal{F}(x, W') G\left(\frac{W - W'}{\sigma_W}\right), \quad (9)$$

where

$\sigma_{R \rightarrow hadr}(W) = \frac{6\pi^2}{M_R^2} \Gamma_{ee}^R \cdot Br(R \rightarrow hadr) \cdot \delta(W - M_R)$ ,  $\sigma_0$  is the nonresonant background cross section,  $\mathcal{F}(x, W)$  is the radiative correction function [21],  $G(x)$  is the Gaussian function.

The likelihood fits are performed with the  $M_R$  varied in 0.1 MeV steps with  $\Gamma_{ee}^R \cdot Br(R \rightarrow hadr)$  as a free parameter, the energy range in the fit for each  $M_R$  value is  $M_R \pm 13 \text{ MeV}$ . The upper limit obtained with this procedure is  $\Gamma_{ee}^R \cdot Br(R \rightarrow hadr) < 100 \text{ eV}$  at 90%

confidence level. In order to get a more conservative upper limit we took into account that:

- $\varepsilon_{J/\psi \rightarrow hadr} / \varepsilon_{e^+e^- \rightarrow hadr}(3.1 \text{ GeV}) \simeq 1.15$ ,
- $\varepsilon_{e^+e^- \rightarrow hadr}(3.1 \text{ GeV}) / \varepsilon_{e^+e^- \rightarrow hadr}(1.9 \text{ GeV}) \simeq 1.2$ ,
- variation of  $\sigma_W$  could further increase the limit.

Combining all the factors, we set a limit

$$\Gamma_{ee}^R \cdot Br(R \rightarrow hadr) < 150 \text{ eV (90 \% c.l.)}$$

in the W range between 1.85 GeV and  $M_{J/\Psi}$ .

## 6 Results

Masses of charged and neutral  $D$  mesons are obtained at KEDR experiment:

- $M_{D^0} = 1865.30 \pm 0.33 \pm 0.23 \text{ MeV}$ ,
- $M_{D^+} = 1869.53 \pm 0.49 \pm 0.20 \text{ MeV}$ .

The  $D^0$  mass value is consistent with the more precise measurement of the CLEO collaboration [27], while

that of the  $D^+$  mass is presently the most precise direct determination.

The preliminary  $\psi(3770)$  parameters are obtained with standard non-interference parameterization [18, 19]:

- $M = 3773.2 \pm 0.5 \pm 0.6 \text{ MeV}$ ,
- $\Gamma_{tot} = 23.9 \pm 2.2 \pm 1.1 \text{ MeV}$ ,
- $\Gamma_{ee} = 294 \pm 22 \pm 30 \text{ eV}$ .

The parameters with the interference:

- $M = 3777.8 \pm 1.1 \pm 0.7 \text{ MeV}$ ,
- $\Gamma_{tot} = 28.2 \pm 3.1 \pm 2.4 \text{ MeV}$ ,
- $\Gamma_{ee} = 312 \pm 31 \pm 30 \text{ eV}$ .

Taking the interference into account significantly improves the fit quality and increases the  $\psi(3770)$  mass by 4.6 MeV.

A preliminary upper limit for narrow resonances in the W range between 1.85 GeV and  $M_{J/\Psi}$ :

- $\Gamma_{ee}^R \cdot Br(R \rightarrow hadr) < 150 \text{ eV (90 \% c.l.)}$ .

## References

- 1 V. Anashin *et al.*, Stockholm 1998, EPAC 98\*, 400 (1998), Prepared for 6th European Particle Accelerator Conference (EPAC 98), Stockholm, Sweden, 22-26 Jun 1998.
- 2 V. E. Blinov *et al.*, Nucl. Instrum. Meth. **A598**, 23 (2009).
- 3 KEDR, V. M. Aulchenko *et al.*, Phys. Lett. B **573**, 63 (2003), arXiv:hep-ex/0306050.
- 4 R. Klein, R. Thornagel, G. Ulm, T. Mayer, and P. Kuske, Nucl. Instrum. Meth. **A384**, 293 (1997).
- 5 R. Klein *et al.*, Nucl. Instrum. Meth. **A486**, 545 (2002).
- 6 V. V. Anashin *et al.*, Nucl. Instrum. Meth. **A478**, 420 (2002).
- 7 Belle Collaboration, S. K. Choi *et al.*, Phys. Rev. Lett. **91**, 262001 (2003).
- 8 CDF Collaboration, D. E. Acosta *et al.*, Phys. Rev. Lett. **93**, 072001 (2004).
- 9 D0 Collaboration, V. M. Abazov *et al.*, Phys. Rev. Lett. **93**, 162002 (2004).
- 10 BaBar Collaboration, B. Aubert *et al.*, Phys. Rev. D **71**, 071103 (2005).
- 11 E. S. Swanson, Phys. Lett. B **588**, 189 (2004).
- 12 T. Sjostrand and M. Bengtsson, Comput. Phys. Commun. **43**, 367 (1987).
- 13 S. E. Avvakumov *et al.*, BINP preprint 2006-038 (in Russian).
- 14 E. Barberio and Z. Was, Comput. Phys. Commun. **79**, 291 (1994).
- 15 Particle Data Group, W.-M. Yao *et al.*, Journal of Physics G **33**, 1 (2006).
- 16 R. Brun *et al.*, CERN Report No. DD/EE/84-1 (1993).
- 17 Particle Data Group, C. Amsler *et al.*, Phys. Lett. B **667**, 1 (2008).
- 18 R.H. Schindler *et al.*, Phys. Rev. D **21**, 2716 (1980).
- 19 M. Ablikim *et al.*, Phys. Rev. Lett. **97** 121801 (2006).
- 20 B. Aubert *et al.*, Phys. Rev. D **76** 111105(R) (2007).
- 21 E.A.Kuraev and V.S.Fadin, Sov.J.Nucl.Phys. **41**, 466 (1985).
- 22 J. Siegrist *et al.*, Phys. Rev. D **26**, 969 (1982).
- 23 B. Nickzuporuk *et al.*, Z. Phys. C - Particles and Fields **15**, 299 (1982).
- 24 A. E. Blinov *et al.*, Z. Phys. C - Particles and Fields **49**, 239 (1991).
- 25 C. Bacci *et al.*, Phys.Lett.B **58**, 481 (1975).
- 26 C. Bacci *et al.*, Phys.Lett.B **64**, 356 (1976).
- 27 CLEO Collaboration, C. Cawfield *et al.*, Phys. Rev. Lett. **98**, 092002 (2007).